NANO LETTERS

pubs.acs.org/NanoLett

Letter

Evidence for Moiré Trions in Twisted $MoSe_2$ Homobilayers

Elizabeth Marcellina, Xue Liu, Zehua Hu, Antonio Fieramosca, Yuqing Huang, Wei Du, Sheng Liu, Jiaxin Zhao, Kenji Watanabe, Takashi Taniguchi, and Qihua Xiong*

Cite This: *Nano Lett.* 2021, 21, 4461−4468

Read Online

ACCESS | Metrics & More | Article Recommendations | Supporting Information

ABSTRACT: Moiré superlattices of van der Waals structures offer a powerful platform for engineering band structure and quantum states. For instance, Moiré superlattices in magic-angle twisted bilayer graphene, ABC trilayer graphene have been shown to harbor correlated insulating and superconducting states, while in transition metal dichalcogenide (TMD) twisted bilayers, Moiré excitons have been identified. Here we show that the effects of a Moiré superlattice on the band structure are general: In TMD twisted bilayers, excitons and exciton complexes can be trapped in the superlattice in a manner analogous to ultracold bosonic or Fermionic atoms in optical lattices. Using twisted $MoSe_2$ homobilayers as a model system, we present evidence for Moiré trions. Our results thus open possibilities for designer van der Waals structures hosting arrays of Fermionic or bosonic quasiparticles, which can be used to realize tunable many-body states crucial for quantum simulation and quantum information processing.

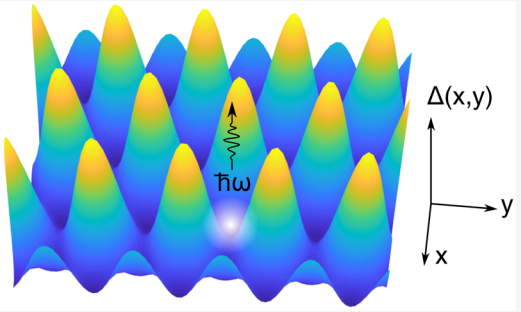

KEYWORDS: *Moiré excitons, Moiré trions, twisted homobilayers, van der Waals heterostructures, transition metal dichalcogenides, two-dimensional materials*

The discovery of two-dimensional materials and their layered van der Waals structures[1,2] has ushered in a new era of functional materials promising a high degree of customization. The wide varieties of atomically thin materials[3] and possible layer combinations, as well as state-of-the-art fabrication techniques, allow one to envisage and realize quantum materials with tailorable "properties on demand".[4] The fertile research field of two-dimensional materials has in the recent years been guided by this framework with the chief goals of discovering new states of matter and phase transitions,[5] solving longstanding problems such as high-T_c superconductivity,[6] creating novel devices that operate on the quantum mechanical principles,[7] and satisfying the interest in fundamental physics.

Recent prominent examples of how stacking two monolayers or more can dramatically alter the electronic properties can be illustrated with Moiré structures, which are fabricated by stacking two or more monolayers at a given twist angle.[8] In Moiré structures, the electronic Bloch bands are modulated with a period defined by the twist angle. Depending on the electrostatic landscape, particles and quasiparticles can be trapped in the Moiré superlattice, where many-body interactions may give rise to correlated quantum states.[9] For instance, in twisted bilayer graphene with a twist angle of 1.1° ("magic angle"),[8,10,11] ABC trilayer graphene,[12−14] and twisted bilayer WSe_2 with twist angles ranging from 4° to 5°,[15] flat electronic bands form and cause the kinetic energy to become quenched. The quenching of the kinetic energy gives rise to many-body states such as correlated insulators,[10,15] unconventional superconductivity,[11] and spontaneous time-reversal symmetry breaking that causes an anomalous Hall effect[16] and quantum anomalous Hall effect.[17]

A Moiré superlattice can also affect the optical properties of materials with a finite band gap, such as in the transition metal dichacolgenides (TMDs). TMD materials are presently attracting a lot of research attention because of their excellent optical properties,[18−21] strong spin−orbit coupling, and a valley pseudospin degree of freedom (along the K and K' directions) that can be optically addressed[22−27] and possesses a nontrivial Berry phase.[24] The Moiré superlattice in TMDs strongly affects the optical properties by introducing different optical selection rules from the constituent monolayers.[28−31] In particular, electrons and holes can trapped in the Moiré superlattice, and they can radiatively recombine to form Moiré excitons.[30−34] As the energies of the Moiré excitons can be finely tuned by means of electrostatic gates and twist angle, the Moiré excitons are thus a promising platform for realizing arrays of quantum emitters,[28] topological excitons,[35] and exciton superfluids.[36,37]

Received: March 26, 2021
Revised: May 5, 2021
Published: May 10, 2021

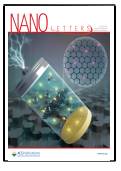

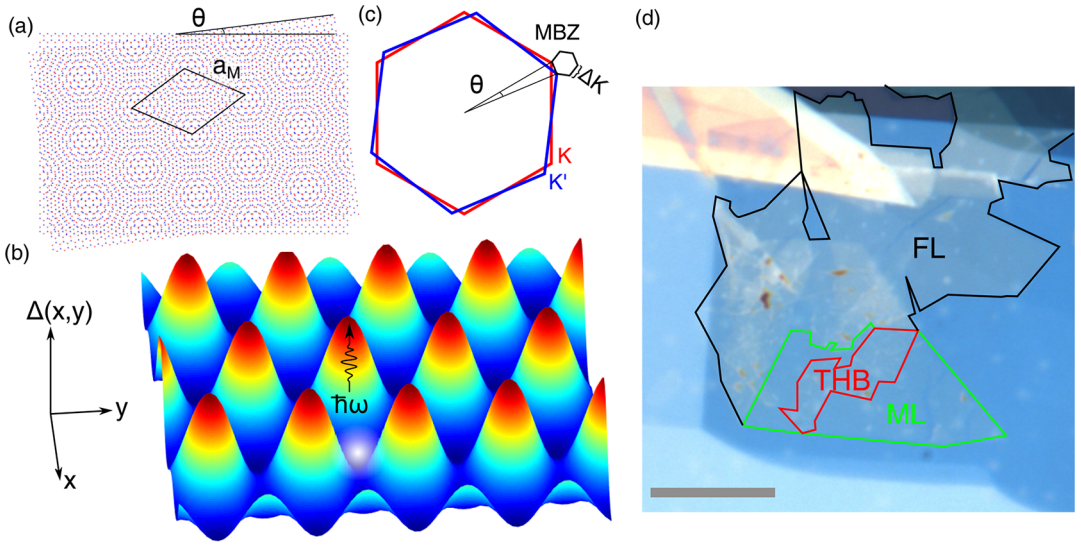

Figure 1. (a) A homobilayer with twist angle θ exhibits a Moiré pattern with period a_M. (b) A Moiré superlattice in (a) causes a periodic modulation in the electrostatic potential of the homobilayer, which can trap quasi-particles (e.g., excitons or exciton complexes, here depicted by an orange sphere) in the periodic potential. (c) The formation of Moiré unit cells causes Moiré Brillouin zones to form. (d) A representative sample image for an aligned (i.e., $\theta = 0°$) twisted homobilayer on hexagonal boron nitride (hBN) on SiO_2/Si. Here FL = few-layer $MoSe_2$, ML = $MoSe_2$ monolayer, and THB = $MoSe_2$ twisted homobilayer. The scale bar is 10 μm.

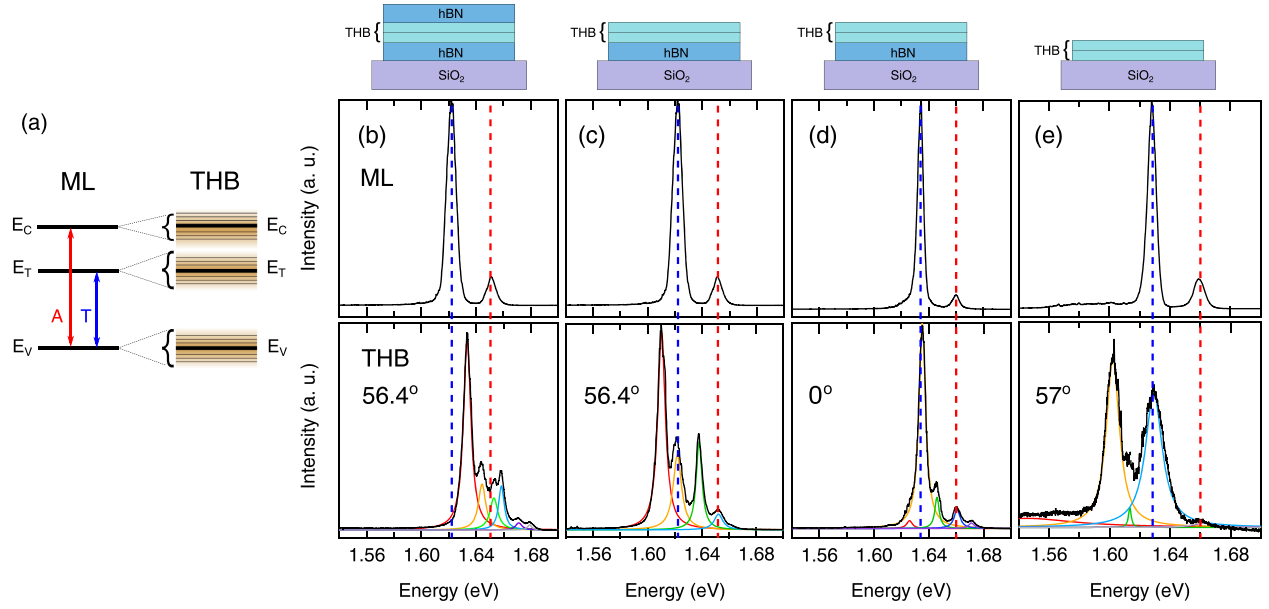

Figure 2. (a) Energy bands of an $MoSe_2$ monolayer (left) and the formation of the Moiré trion and exciton subbands (with the energy levels not to scale) in a twisted homobilayer (right). In a twisted homobilayer, the additional energy levels allow optical transitions with energies different to those in the monolayer. Here, E_c, E_v, and E_T refer to conduction band, valence band, and trion energy levels of the monolayer, respectively. The photoluminescence from (b) an aligned homobilayer that is encapsulated with hBN, (c,d) homobilayers that are transferred on hBN (no top hBN), and (e) an unencapsulated twisted homobilayer. In all these homobilayers, the most prominent photoluminescence comes from the energies closest to the monolayer trions. The blue (red) dashed lines in panels (b−d) correspond to the monolayer trion (exciton) photoluminescence energy. The temperature for the measurements in (b−d) is 5 K.

The optically active states of TMDs are not limited to excitons but can also exist as exciton complexes such as trions,[38−40] neutral biexcitons,[41,42] and charged biexcitons.[39,42] Because exciton complexes can be fermions or bosons, exciton complexes in Moiré structures may be the solid-state analogues of ultracold Fermionic atoms,[43] ultracold bosonic atoms,[44] and neutral atoms with artificial gauge fields[45] in optical lattices, all of which are the standard tools of trade for quantum simulation.[46] It is thus our goal to demonstrate that it is possible to create Moiré structures with exciton complexes, since they will expand the possibilities for quantum simulations with TMDs.[47−49] With this motivation, we show in this work evidence for Moiré trions using twisted $MoSe_2$ homobilayers as a model system.

We now describe in detail how a Moiré superlattice defines the electronic states and the corresponding optical transitions. Figure 1a presents an illustration of a Moiré superlattice characterized with a period of $a_M = a/(2\sin[\theta/2])$ that forms

https://doi.org/10.1021/acs.nanolett.1c01207
Nano Lett. 2021, 21, 4461−4468

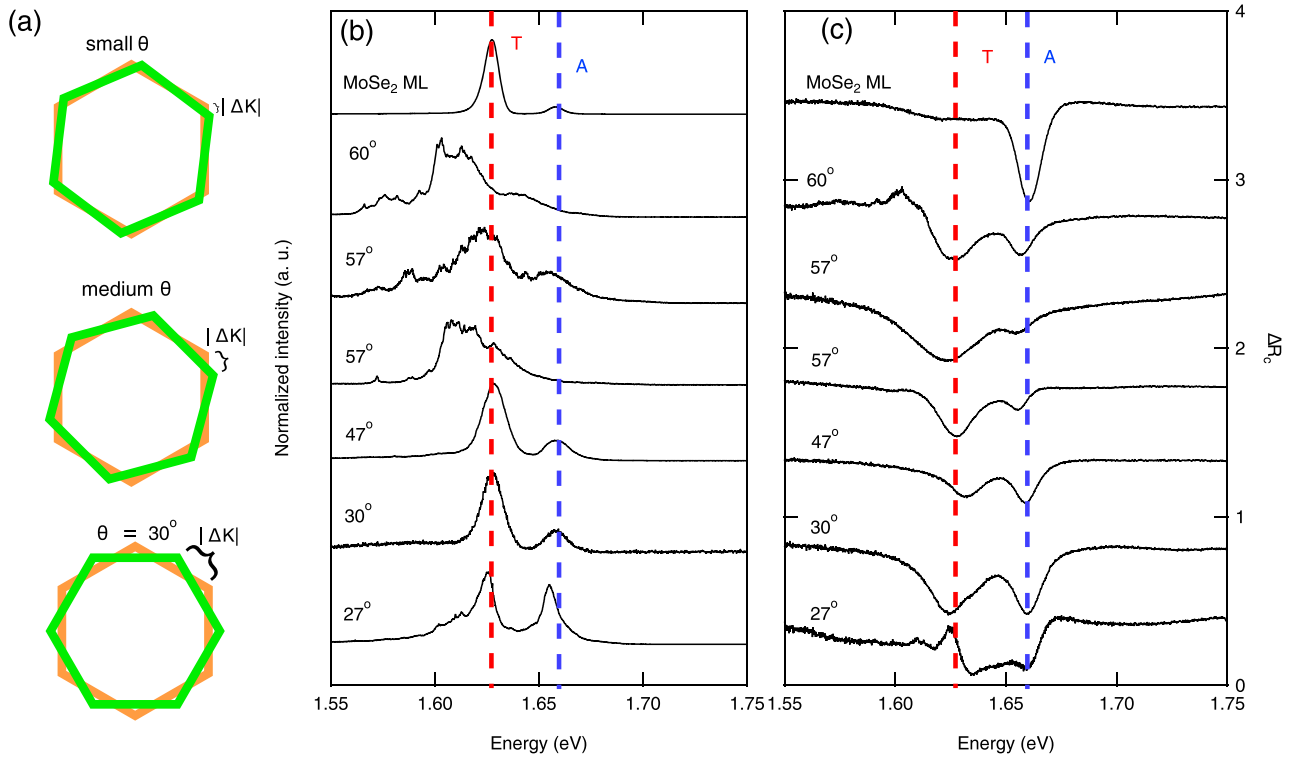

Figure 3. (a) An illustration of the Brillouin zone of the bottom and top layers for small and medium twist angles, as well as 30°. At small (large) twist angles, each pair of top K (or K') and bottom K' (or K) valleys are strongly (weakly) coupled and the optical dipole transition is strong (weak).[50] (b) Photoluminescence spectra for twisted homobilayers with various twist angles. (c) The reflectance contrast $\Delta R_c \equiv (R - R_0)/R_0$ for the samples in (c), where R (R_0) is the reflectance of the sample (substrate). The traces are offset for clarity. The blue (red) dashed lines in panels (b) and (c) correspond to the monolayer trion (exciton) photoluminescence energy. The temperature is kept at 5 K.

when two monolayers of the same material are stacked on top of each other with a twist angle θ, where a is the monolayer lattice constant. Figure 1b is a schematic of a spatially periodic confinement potential that arises from the Moiré superlattice. This spatially periodic potential $\Delta(\boldsymbol{r}) \equiv \Delta(x, y)$ modulates the unperturbed electronic bands of the monolayers and hence alters the electronic structures of the Moiré bilayers in the out-of-plane and in-plane directions. The confinement potential defines the energy levels of the system at zero in-plane momentum. Therefore, depending on the electrostatic landscape, electrons or holes, as well as light-excited quasiparticles such as excitons and exciton complexes (depicted by the orange sphere) can become trapped in the potential. In the momentum space, an additional set of Brillouin zones (which are termed as Moiré Brillouin zones) of size $|\Delta K| = 4\pi/(\sqrt{3}\,a_M)$ form (Figure 1c). The energy-momentum dispersion of a Moiré superlattice can be described by Bloch bands with period characterized by the Moiré unit cell a_M.[8] The size of the Brillouin zone defines the occupation number of a Moiré unit cell and the optical transition dipole strength.[50] In Figure 1d, we show a representative image of a twisted $MoSe_2$ homobilayer, which was made by stacking two $MoSe_2$ monolayers with a twist angle of 0°.

The formation of the Moiré Brillouin zone in Figure 1c causes new energy subbands to form in twisted bilayers with twist angles close to 0° or 60° (Figure 2a). In Figure 2b–d, we show a representative photoluminescence spetrum of $MoSe_2$ monolayers (top panels) as well as twisted $MoSe_2$ homobilayers (bottom panels) with small twist angles $\theta \approx 0°$ or $\theta \approx 60°$ at a temperature of 5 K (solid black lines). The photoluminescence spectrum of the monolayer is well-known[51] with a free excitons peak (or A excitons, denoted by the red dashed lines) and a trions peak (denoted by the dashed blue lines) with a binding energy of 30 meV with respect to the A excitons peak. For the twisted homobilayers, optical transitions also occur at slightly different energies as compared with the trions and free excitons peaks, as a result of subband formation that ensues from the Moiré Brillouin zone. In Figure 2b–d the formation of multiple light-excited quasiparticle subbands can be clearly observed (red, yellow, green, blue, and purple lines), which indicate the presence of a Moiré superlattice in our samples. The subbands are most clearly resolved in the encapsulated sample (fwhm ≈ 5–6 meV), followed with the twisted homobilayers on a bottom hBN (fwhm ≈ 6–7 meV) and the unencapsulated twisted homobilayer (fwhm ≈ 10–15 meV).

We now associate the energy spacing of the trions in Figure 2b–e to the Moiré potential using perturbation theory. The typical energy spacing for trion subbands in Figure 2b–e is 11 meV. For small twist angles, the trion subband energy spacings can be mapped to the energy level spacing of a harmonic oscillator.[29,30] The Hamiltonian for the Moiré system is given as[29]

$$H = E_0 + \frac{\hbar^2\kappa^2}{2M} + \Delta(\mathbf{r}) \tag{1}$$

$$\Delta(\mathbf{r}) = 2V\Sigma_{j=1,3,5}\cos(\mathbf{b}_j.\,\mathbf{r} - \psi) \tag{2}$$

where E_0 is the energy of the Bloch band at zero in-plane momentum, κ is the in-plane wave vector, $\Delta(\boldsymbol{r})$ is the Moiré potential, V is a constant, $\boldsymbol{b}_j$ represents the Moiré Brillouin zone 3-fold rotation symmetric unit vectors, and ψ is a phase.[30]

https://doi.org/10.1021/acs.nanolett.1c01207
Nano Lett. 2021, 21, 4461–4468

We choose the phase ϕ to be π so that the $\Delta(r)$ is minimum at the AA site. The potential $\Delta(r)$ can thus be approximated as a harmonic oscillator potential so that $\Delta(\mathbf{r}) = -6V + 16\pi^2 V(\mathbf{r}/a_M)^2/2$.[30] Using this harmonic oscillator model, we can calculate the potential depth of the Moiré potential and the number of subbands within the harmonic potential. For a twist angle of 1° and 59°, the Moiré period a_M of 18.9 nm and $MoSe_2$ trion effective mass of $M = 2m_e + m_h$,[51] where $m_e = 0.6\ m_0$ and $m_h = 0.6\ m_0$ are the effective masses of electrons and holes in $MoSe_2$ respectively,[52] we find V to be $V = 7$ meV and the peak to peak difference $V_{pp} = 9V$ of the Moiré potential to be V_{pp} meV, which is sufficiently deep to split the trion band into subbands separated by 11 meV. We now consider larger twist angles. For a twist angle of 2° and 58°, the Moiré period a_M reduces to 10 nm, and for a subband spacing of 11 meV, we find $V = 1.7$ meV and the depth of the Moiré potential is $V_{pp} = 9V = 15.3$ meV, which is also sufficiently deep to cause trion subband formation with an energy spacing of 11 meV. For a twist angle of 3° and 57°, we find $V = 0.8$ meV and the depth of the Moiré potential is $V_{pp} = 9V = 7.2$ meV. While the harmonic potential model gives a good agreement with our observed energy subband spacing of 11 meV for twist angles of 1°, 2°, 58°, and 59°, for twist angles θ or $(60° - \theta)$ with $\theta \gtrsim 3°$, the simple harmonic potential model is no longer accurate. In order to associate the observed energy spacing of 11 meV to the Moiré superlattice at twist angles $\theta \gtrsim 3°$ or $(60° - \theta)$, one has to consider the transition between highly localized states into more delocalized states,[53] and higher-order terms in the perturbation expansion need to be considered. However, despite the limitations of the simple harmonic potential model of the Moiré potential, this model correctly predicts the order of magnitude of the energy spacings in homobilayers with small twist angles of the Moiré subbands and potential depth. (Note: Another physical phenomenon that can also cause multiple photoluminescence peaks separated by a regular energy spacing is phonon-assisted photoluminescence that gives rise to phonon replicas. However, this mechanism is unlikely the origin of the multiple peaks observed in our samples, as phonon replicas are typically separated by ~20 meV.[54])

To provide another piece of evidence that the subbands in aligned twisted homobilayers such as those in Figure 2b–d are due to the Moiré potential, we fabricated and measured 7 other encapsulated twisted homobilayers with various twist angles. Figure 3a illustrates the orientation of the Brillouin zone of each monolayer for small, medium, and large twist angles. At small twist angles, $|\Delta K|$ is small and optical transition between the two layers is more probable, whereas at large twist angles, $|\Delta K|$ is large and optical transition between the two layers is less probable as in this case an optical transition requires a large phonon momentum. We now examine the twist angle dependence of the photoluminescence spectra (Figure 3b). At small twist angles (i.e., 60° and 57°), the optical transition dipole moment is large[50] and radiative transitions are probable, which explains the optical transitions at different emission energies from the trions and A excitons in the monolayer. At twist angles of 27°, 30° 47°, the size $|\Delta K|$ of the Moiré Brillouin zone is larger than that of the aligned twisted homobilayers. Consequently, the optical transitions with energies different than the trions and A excitons is suppressed so that the possible optical transitions follow those of the individual monolayers. Figure 3c shows the reflectance contrast $\Delta R_c \equiv \frac{R - R_0}{R_0}$, where R and R_0 are the sample and background reflectance respectively, for the monolayer samples and the homobilayers with various twist angles. For all the twisted homobilayers, reflectance measurement shows that the trion absorption is always enhanced as compared with that of the monolayer, regardless of the twist angle. The enhancement of the trion reflectance indicates increased occupation of the trion subbands in twisted homobilayers. (Note: We also measured the reflectance of the sample in Figure 2c and found the results to be consistent in that in the twisted homobilayer part of the sample, the trion reflectance was again enhanced, as shown in Figure S1.) Combining the fact that the trion reflectance is enhanced in the twisted homobilayers, and that only the aligned homobilayers show photoluminescence with emission energies around that of the monolayer trions, we conclude that the optical transitions for the small twist angles (close to 0° and 60°) are due to the formation of Moiré trions rather than Moiré excitons.

We now investigate the linear polarization of one of our aligned twisted homobilayers in order to test how close our sample is to being an ideal Moiré superlattice. An ideal Moiré superlattice has a 3-fold rotational symmetry (with symmetry operations described by the point group C_3), and it has an equal number of sites that emit copolarized and cross-polarized lights.[28,29] Therefore, when an ideal Moiré superlattice is excited with linearly polarized light (which in itself a superposition of an equal amount of right and light polarized lights), the emitted light will not be affected by the direction of the linear polarization. We carried out out this test on an $MoSe_2$ monolayer first to calibrate our measurements. We took the photoluminescence of the monolayer as a function of the linear polarization direction ϕ with respect to the polarizer (Figure 4a). As the monolayer has a 3-fold rotational symmetry, the monolayer photoluminescence does not exhibit a linear polarization (Figure S2a). We then repeated this measurement with an uncapsulated twisted homobilayer (i.e., the first 57° sample in Figure 3b). Figure 4b shows the linear polarization dependence of the twisted homobilayer, whose photoluminscence is slightly affected by the linear polarization (Supplementary Figure S2c,d). In fact, the highest degree of linear polarization in our sample (Figure 4b) was around (33 ± 17)% at the emission energy of 1.55 eV, while the lowest was around (18 ± 9)% at the emission energy of 1.65 eV (see Supplementary Figure S3a–f for detailed characterizations). The deviation from the C_3 symmetry in the homobilayer is very likely due to strain,[34,55,56] which causes an unequal distribution of sites emitting co- and cross-polarized lights.[34] However, the degree of linear polarization in our twisted homobilayer is still much lower than strained heterostructures reported in the literature, where the linear polarization can reach up to 60–90%.[56] This means that in our sample, the C_3 symmetry is generally preserved so that the shape of the Moiré superlattice is largely regular.

Lastly, we performed angle-resolved photoluminescence (Figure S4) and lifetime measurements (Figure S5) on the twisted homobilayer in Figure 2c. Angle-resolved photoluminescence measurements[57,58] reveal an in-plane dipole orientation, which again support the interpretation that the subbands around 1.61 eV are *intralayer* trions and they are not *interlayer* excitons. Lifetime measurements also show longer lifetimes τ of the subbands in the twisted homobilayer, where we found $\tau = (147.0 \pm 0.1)$ ps and $\tau = (63.0 \pm 0.1)$ ps for the

https://doi.org/10.1021/acs.nanolett.1c01207
Nano Lett. 2021, 21, 4461–4468

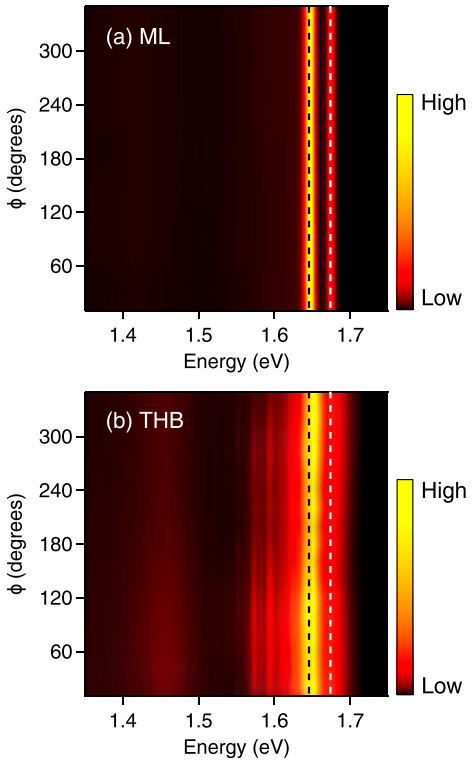

Figure 4. Photoluminescence spectra of an $MoSe_2$ (a) monolayer and (b) twisted homobilayer with twist angle 57°. Here, the angle ϕ is measured between the laser polarization axis and the fast axis of a half-wave plate. The dashed lines correspond to the trion and A exciton peaks of an $MoSe_2$ monolayer. Here, the temperature is 5 K. See text for detailed explanation.

subbands at 1.61 eV and 1.63 respectively, whereas for the monolayer we found $\tau = (82.0 \pm 0.1)$ ps and $\tau = (15.8 \pm 0.1)$ ps for the trions and excitons. These indicate that the subbands in the twisted homobilayer are more localized than the trions and excitons in the monolayer,[59] where this localization is a consistent consequence of the Moiré potential. Moreover, since the lifetime of the subband at 1.61 eV in the homobilayer is longer than the subband at 1.63 eV, it is much more likely that the former corresponds to Moiré trions rather than excitons.

In summary, we have presented experimental evidence for Moiré trions in $MoSe_2$ twisted homobilayers. We identified the Moiré trions through the subband formation in the aligned twisted homobilayers with emission energies close to the monolayer trions. These subbands disappear at large twist angles. We also found that in the twisted homobilayers, the trion reflectance is enhanced compared with the monolayer, which suggests occupation of the trion subbands in the twisted homobilayers. Furthermore, measurements of the linear polarization, angle-resolved photoluminescence, and lifetime in the aligned twisted homobilayers also corroborate the interpretation of Moiré trions. Finally, we expect that this work will stimulate further investigations on Moiré exciton complexes in TMDs, which can in turn be used as platforms for realizing exotic phases such as correlated many-body phases, quantum simulators, arrays of identical quantum emitters, topological excitons, and Moiré polaritons.

METHODS

Sample Preparation. We used *n*-doped $MoSe_2$ crystals purchased from HQ Graphene for exfoliation. The homobilayers were fabricated by stacking mechanically exfoliated $MoSe_2$ monolayers using a dry-transfer technique[60] with a polydimethylsiloxane (PDMS) stamp. The bottom monolayer was first transferred onto silicon substrates coated with a 100 nm SiO_2 wafer. The top $MoSe_2$ monolayer was then stacked onto the bottom monolayer with the crystal axes rotationally aligned under an optical microscope. After stacking the two monolayers, the samples were annealed in high vacuum ($<10^{-5}$ mbar) at 120° for 1 h.

Optical Spectroscopy Measurements. *Steady-State Photoluminescence Measurements.* The steady-state photoluminescence measurements in Figures 2−4 were performed at a temperature of 5 K using a continuous-wave 633 nm laser focused to a spot size of 1 μm with a 50× (NA = 0.50) objective. For the reflectivity measurements, we used a broadband white light source for light excitation. The transmitted signals were then dispersed by a diffraction grating (600 lines/mm) through a spectrometer (Horiba-JY HR800) and detected by a liquid nitrogen-cooled charge-coupled device (Horiba Symphony II).

Angle-Resolved Photoluminescence Measurements. The angle-resolved photoluminescence measurements were performed in a home-built setup with a Fourier imaging configuration. A high numerical aperture 100× microscope objective (NA = 0.75) was used in our angle-resolved measurements, which covered an angular range of ±48.6°. The emission from the sample was collected through the narrow entrance slit of the spectrometer (Horiba-JY iHR550) and finally onto a liquid nitrogen-cooled charge-coupled device (Horiba Symphony II).

Time-Resolved Photoluminescence Measurements. The time-resolved photoluminescence spectroscopy measurement was performed with a home-built confocal microphotoluminescence setup. Throughout the measurements, the samples were mounted in a continuous flow optical cryostat. A Ti:sapphire femtosecond laser with ∼100 fs pulse duration and a repetition rate of 80 MHz was used as the excitation source. The laser excitation wavelength was 800 nm and was frequency-doubled to 400 nm. The time-resolved photoluminescence emission is resolved with a spectrometer (Horiba-JY iHR320) and detected by a charge-coupled device (Horiba Symphony II). The photons exiting the spectrometer were then detected with an avalanche detector connected to a single-photon counting module (PicoHarp 300). The average excitation power of the pulsed laser was ∼2.5 μW.

Second Harmonic Generation Measurements. The twist angles were determined using second harmonic generation (SHG) with the pulsed the above-mentioned Ti:sapphire femtosecond laser. We rotated the sample with respect to the laser polarization and collected the emission at 400 nm for each sample orientation. The result was fitted to $I(\theta) = I_0 \cos^2(3\cos\theta + 2\eta)$, where I_0 is the maximum SHG intensity, η the initial angle between the crystal armchair axis and the laser polarization, θ is the angle between the crystal armchair axis and η,[61] and I is the collected SHG intensity. Since the function $I = I_0 \cos^2(3\cos\theta + 2\eta)$ has a 6-fold symmetry and does not discriminate between a twist angle of 0° and 60° between the monolayers, we took an additional step to determine the relative crystal orientation between the

https://doi.org/10.1021/acs.nanolett.1c01207
Nano Lett. 2021, 21, 4461−4468

monolayers. To this end, we compared the SHG intensity of each monolayers and their twisted bilayer: if the SHG intensity of the twisted bilayer is stronger than (weaker than or in between) that of each monolayers, the SHG response in the twisted bilayer is a constructive (destructive) interference of the response of each monolayer and the twist angle between the monolayers is close to 0° (60°).[62] A representative data set of SHG measurements are shown in Supplementary Figure S6a,b.

■ ASSOCIATED CONTENT

Supporting Information

The Supporting Information is available free of charge at https://pubs.acs.org/doi/10.1021/acs.nanolett.1c01207.

Additional low-temperature optical measurements and second-harmonic generation (PDF)

■ AUTHOR INFORMATION

Corresponding Author

Qihua Xiong − *State Key Laboratory of Low-Dimensional Quantum Physics and Department of Physics, Tsinghua University, Beijing 100084, P.R. China; Beijing Academy of Quantum Information Sciences, Beijing 100193, P.R. China;* orcid.org/0000-0002-2555-4363; Email: qihua_xiong@tsinghua.edu.cn

Authors

Elizabeth Marcellina − *School of Physical and Mathematical Sciences, Nanyang Technological University, Singapore 637371*

Xue Liu − *School of Physical and Mathematical Sciences, Nanyang Technological University, Singapore 637371*

Zehua Hu − *School of Physical and Mathematical Sciences, Nanyang Technological University, Singapore 637371;* orcid.org/0000-0002-1185-2992

Antonio Fieramosca − *School of Physical and Mathematical Sciences, Nanyang Technological University, Singapore 637371*

Yuqing Huang − *School of Physical and Mathematical Sciences, Nanyang Technological University, Singapore 637371*

Wei Du − *School of Physical and Mathematical Sciences, Nanyang Technological University, Singapore 637371;* orcid.org/0000-0001-8678-8844

Sheng Liu − *School of Physical and Mathematical Sciences, Nanyang Technological University, Singapore 637371*

Jiaxin Zhao − *School of Physical and Mathematical Sciences, Nanyang Technological University, Singapore 637371*

Kenji Watanabe − *Research Center for Functional Materials, National Institute for Materials Science, Tsukuba, Ibaraki 305-0044, Japan;* orcid.org/0000-0003-3701-8119

Takashi Taniguchi − *International Center for Materials Nanoarchitectonics, National Institute for Materials Science, Tsukuba, Ibaraki 305-0044, Japan;* orcid.org/0000-0002-1467-3105

Complete contact information is available at: https://pubs.acs.org/10.1021/acs.nanolett.1c01207

Author Contributions

Q.X. supervised the project. E.M. conceived the idea, designed the experiments, fabricated the samples, performed the measurements, and wrote the manuscript. X.L. and Z.H. helped with the sample preparation. A.F. helped with the angle-resolved photoluminescence measurements. Y.H. helped with the lifetime measurements. A.F., W.D., J.Z., and S.L. helped with and advised on the second harmonic generation measurements. K.W. and T.T. provided the hBN crystals.

Notes

The authors declare no competing financial interest.

■ ACKNOWLEDGMENTS

We acknowledge the support from the Singapore Ministry of Education via AcRF Tier 3 Programme "Geometrical Quantum Materials" (MOE2018-T3-1-002). Q.X. gratefully acknowledges National Natural Science Foundation of China (No. 12020101003) and start-up grant from Tsinghua University. K.W. and T.T. acknowledge support from the Elemental Strategy Initiative conducted by the MEXT, Japan (grant number JPMXP0112101001), JSPS KAKENHI (grant number JP20H00354) and the CREST(JPMJCR15F3), JST.

■ REFERENCES

(1) Geim, A. K.; Grigorieva, I. V. van der Waals heterostructures. *Nature* **2013**, *499*, 419−425.

(2) Novoselov, K. S.; Mishchenko, A.; Carvalho, A.; Castro Neto, A. H. 2D materials and van der Waals heterostructures. *Science* **2016**, *353*, aac9439.

(3) Zhou, J.; et al. A library of atomically thin metal chalcogenides. *Nature* **2018**, *556*, 355.

(4) Basov, D. N.; Averitt, R. D.; Hsieh, D. Towards properties on demand in quantum materials. *Nat. Mater.* **2017**, *16*, 1077−1088.

(5) Vojta, M. Quantum phase transitions. *Rep. Prog. Phys.* **2003**, *66*, 2069.

(6) Keimer, B.; Kivelson, S. A.; Norman, M. R.; Uchida, S.; Zaanen, J. From quantum matter to high-temperature superconductivity in copper oxides. *Nature* **2015**, *518*, 179−186.

(7) Tokura, Y.; Kawasaki, M.; Nagaosa, N. Emergent functions of quantum materials. *Nat. Phys.* **2017**, *13*, 1056−1068.

(8) Bistritzer, R.; MacDonald, A. H. Moiré bands in twisted double-layer graphene. *Proc. Natl. Acad. Sci. U. S. A.* **2011**, *108*, 12233−12237.

(9) Koshino, M.; Yuan, N. F. Q.; Koretsune, T.; Ochi, M.; Kuroki, K.; Fu, L. Maximally Localized Wannier Orbitals and the Extended Hubbard Model for Twisted Bilayer Graphene. *Phys. Rev. X* **2018**, *8*, 031087.

(10) Cao, Y.; Fatemi, V.; Demir, A.; Fang, S.; Tomarken, S. L.; Luo, J. Y.; Sanchez-Yamagishi, J. D.; Watanabe, K.; Taniguchi, T.; Kaxiras, E.; Ashoori, R. C.; Jarillo-Herrero, P. Correlated insulator behaviour at half-filling in magic-angle graphene superlattices. *Nature* **2018**, *556*, 80−84.

(11) Cao, Y.; Fatemi, V.; Fang, S.; Watanabe, K.; Taniguchi, T.; Kaxiras, E.; Jarillo-Herrero, P. Unconventional superconductivity in magic-angle graphene superlattices. *Nature* **2018**, *556*, 43−50.

(12) Chen, G.; Jiang, L.; Wu, S.; Lyu, B.; Li, H.; Chittari, B. L.; Watanabe, K.; Taniguchi, T.; Shi, Z.; Jung, J.; Zhang, Y.; Wang, F. Evidence of a gate-tunable Mott insulator in a trilayer graphene moiré superlattice. *Nat. Phys.* **2019**, *15*, 237−241.

(13) Chen, G.; Sharpe, A. L.; Gallagher, P.; Rosen, I. T.; Fox, E. J.; Jiang, L.; Wu, S.; Lyu, B.; Li, H.; Watanabe, K.; Taniguchi, T.; Jung, Z.; Shi, Z.; Goldhaber-Gordon, D.; Zhang, Y.; Wang, F. Signatures of tunable superconductivity in a trilayer graphene moiré superlattice. *Nature* **2019**, *572*, 215.

(14) Chen, G.; et al. Tunable correlated Chern insulator and ferromagnetism in a moiré superlattice. *Nature* **2020**, *579*, 56.

(15) Wang, L.; et al. Correlated electronic phases in twisted bilayer transition metal dichalcogenides. *Nat. Mater.* **2020**, *19*, 861−867.

(16) Sharpe, A. L.; Fox, E. J.; Barnard, A. W.; Finney, J.; Watanabe, K.; Taniguchi, T.; Kastner, M. A.; Goldhaber-Gordon, D. Emergent

ferromagnetism near three-quarters filling in twisted bilayer graphene. *Science* **2019**, *365*, 605−608.
(17) Serlin, M.; Tschirhart, C. L.; Polshyn, H.; Zhang, Y.; Zhu, J.; Watanabe, K.; Taniguchi, T.; Balents, L.; Young, A. F. Intrinsic quantized anomalous Hall effect in a moiré heterostructure. *Science* **2020**, *367*, 900−903.
(18) Chernikov, A.; Berkelbach, T. C.; Hill, H. M.; Rigosi, A.; Li, Y.; Aslan, O. B.; Reichman, D. R.; Hybertsen, M. S.; Heinz, T. F. Exciton Binding Energy and Nonhydrogenic Rydberg Series in Monolayer WS_2. *Phys. Rev. Lett.* **2014**, *113*, 076802.
(19) Ugeda, M. M.; Bradley, A. J.; Shi, S.-F.; da Jornada, F. H.; Zhang, Y.; Qiu, D. Y.; Ruan, W.; Mo, S.-K.; Hussain, Z.; Shen, Z.-X.; Wang, F.; Louie, S. G.; Crommie, M. F. Giant bandgap renormalization and excitonic effects in a monolayer transition metal dichalcogenide semiconductor. *Nat. Mater.* **2014**, *13*, 1091.
(20) He, K.; Kumar, N.; Zhao, L.; Wang, Z.; Mak, K. F.; Zhao, H.; Shan, J. Tightly Bound Excitons in Monolayer WSe_2. *Phys. Rev. Lett.* **2014**, *113*, 026803.
(21) Wilson, R.; Nguyen, P. V.; Seyler, K.; Rivera, P.; Marsden, A. J.; Laker, Z. P.; Constantinescu, G. C.; Kandyba, V.; Barinov, A.; Hine, D. M.; Xu, X.; Cobden, D. H. Determination of band offsets, hybridization, and exciton binding in 2D semiconductor heterostructures. *Sci. Adv.* **2017**, *3*, e1601832.
(22) Xiao, D.; Yao, W.; Niu, Q. Valley-contrasting physics in graphene: Magnetic moment and topological transport. *Phys. Rev. Lett.* **2007**, *99*, 236809.
(23) Zeng, H.; Dai, J.; Yao, W.; Xiao, D.; Cui, X. Valley polarization in MoS2 monolayers by optical pumping. *Nat. Nanotechnol.* **2012**, *7*, 490−493.
(24) Xiao, D.; Liu, G. B.; Feng, W.; Xu, X.; Yao, W. Coupled spin and valley physics in monolayers of MoS_2 and other group-VI dichalcogenides. *Phys. Rev. Lett.* **2012**, *108*, 196802.
(25) Mak, K. F.; McGill, K. L.; Park, J.; McEuen, P. L. The valley hall effect in MoS_2 transistors. *Science* **2014**, *344*, 1489−1492.
(26) Lee, J.; Wang, Z.; Xie, H.; Mak, K. F.; Shan, J. Valley magnetoelectricity in single-layer MoS_2. *Nat. Mater.* **2017**, *16*, 887−891.
(27) Barré, E.; Incorvia, J. A. C.; Kim, S. H.; McClellan, C. J.; Pop, E.; Wong, H. S.; Heinz, T. F. Spatial Separation of Carrier Spin by the Valley Hall Effect in Monolayer WSe_2 Transistors. *Nano Lett.* **2019**, *19*, 770−774.
(28) Yu, H.; Liu, G. B.; Tang, J.; Xu, X.; Yao, W. Moiré excitons: From programmable quantum emitter arrays to spin-orbit−coupled artificial lattices. *Sci. Adv.* **2017**, *3*, e1701696.
(29) Wu, F.; Lovorn, T.; MacDonald, A. H. Theory of optical absorption by interlayer excitons in transition metal dichalcogenide heterobilayers. *Phys. Rev. B: Condens. Matter Mater. Phys.* **2018**, *97*, 035306.
(30) Tran, K.; et al. Evidence for moiré excitons in van der Waals heterostructures. *Nature* **2019**, *567*, 71−75.
(31) Jin, C.; Regan, E. C.; Yan, A.; Iqbal Bakti Utama, M.; Wang, D.; Zhao, S.; Qin, Y.; Yang, S.; Zheng, Z.; Shi, S.; Watanabe, K.; Taniguchi, T.; Tongay, S.; Zettl, A.; Wang, F. Observation of moiré excitons in WSe_2/WS_2 heterostructure superlattices. *Nature* **2019**, *567*, 76−80.
(32) Seyler, K. L.; Rivera, P.; Yu, H.; Wilson, N. P.; Ray, E. L.; Mandrus, D. G.; Yan, J.; Yao, W.; Xu, X. Signatures of moiré-trapped valley excitons in $MoSe_2/WSe_2$ heterobilayers. *Nature* **2019**, *567*, 66−70.
(33) Alexeev, E. M.; et al. Resonantly hybridized excitons in moiré superlattices in van der Waals heterostructures. *Nature* **2019**, *567*, 81−86.
(34) Sung, J.; et al. Broken mirror symmetry in excitonic response of reconstructed domains in twisted $MoSe_2/MoSe_2$ bilayers. *Nat. Nanotechnol.* **2020**, *15*, 750−754.
(35) Wu, F.; Lovorn, T.; MacDonald, A. H. Topological Exciton Bands in Moire Heterojunctions. *Phys. Rev. Lett.* **2017**, *118*, 147401.
(36) Fogler, M. M.; Butov, L. V.; Novoselov, K. S. High-temperature superfluidity with indirect excitons in van der Waals heterostructures. *Nat. Commun.* **2014**, *5*, 4555.
(37) Zhu, Q.; Tu, M. W.-Y.; Tong, Q.; Yao, W. Gate tuning from exciton superfluid to quantum anomalous Hall in van der Waals heterobilayer. *Sci. Adv.* **2019**, *5*, eaau6120.
(38) Mak, K. F.; He, K.; Lee, C.; Lee, G. H.; Hone, J.; Heinz, T. F.; Shan, J. Tightly bound trions in monolayer MoS_2. *Nat. Mater.* **2013**, *12*, 207−211.
(39) Hao, K.; Specht, J. F.; Nagler, P.; Xu, L.; Tran, K.; Singh, A.; Dass, C. K.; Schüller, C.; Korn, T.; Richter, M.; Knorr, A.; Li, X.; Moody, G. Neutral and charged inter-valley biexcitons in monolayer $MoSe_2$. *Nat. Commun.* **2017**, *8*, 15552.
(40) Lyons, T. P.; Dufferwiel, S.; Brooks, M.; Withers, F.; Taniguchi, T.; Watanabe, K.; Novoselov, K. S.; Burkard, G.; Tartakovskii, A. I. The valley Zeeman effect in inter- and intra-valley trions in monolayer WSe_2. *Nat. Commun.* **2019**, *10*, 2330.
(41) You, Y.; Zhang, X. X.; Berkelbach, T. C.; Hybertsen, M. S.; Reichman, D. R.; Heinz, T. F. Observation of biexcitons in monolayer WSe_2. *Nat. Phys.* **2015**, *11*, 477.
(42) Paur, M.; Molina-Mendoza, A. J.; Bratschitsch, R.; Watanabe, K.; Taniguchi, T.; Mueller, T. Electroluminescence from multi-particle exciton complexes in transition metal dichalcogenide semiconductors. *Nat. Commun.* **2019**, *10*, 1709.
(43) Zwierlein, M. W.; Schunck, C. H.; Schirotzek, A.; Ketterle, W. Direct Observation of the Superfluid Phase Transition in Ultracold Fermi Gases. *Nature* **2006**, *442*, 54−58.
(44) Jaksch, D.; Bruder, C.; Cirac, J. I.; Gardiner, C. W.; Zoller, P. Cold Bosonic Atoms in Optical Lattices. *Phys. Rev. Lett.* **1998**, *81*, 3108−3111.
(45) Lin, Y.-J.; Compton, R. L.; Jimenez-Garcia, K.; Porto, J. V.; Spielman, I. B. Synthetic magnetic fields for ultracold neutral atoms. *Nature* **2009**, *462*, 628−632.
(46) Gross, C.; Bloch, I. Quantum simulations with ultracold atoms in optical lattices. *Science* **2017**, *357*, 995−1001.
(47) Regan, E. C.; et al. Mott and generalized Wigner crystal states in WSe_2/WS_2 moiré superlattices. *Nature* **2020**, *579*, 359.
(48) Tang, Y.; Li, L.; Li, T.; Xu, Y.; Liu, S.; Barmak, K.; Watanabe, K.; Taniguchi, T.; MacDonald, A. H.; Shan, J.; Mak, K. F. Simulation of Hubbard model physics in WSe_2/WS_2 moiré superlattices. *Nature* **2020**, *579*, 353.
(49) Shimazaki, Y.; Schwartz, I.; Watanabe, K.; Taniguchi, T.; Kroner, M.; Imamoglu, A. Strongly correlated electrons and hybrid excitons in a moiré heterostructure. *Nature* **2020**, *580*, 472−477.
(50) Yu, H.; Wang, Y.; Tong, Q.; Xu, X.; Yao, W. Anomalous Light Cones and Valley Optical Selection Rules of Interlayer Excitons in Twisted Heterobilayers. *Phys. Rev. Lett.* **2015**, *115*, 187002.
(51) Ross, J. S.; Wu, S.; Yu, H.; Ghimire, N. J.; Jones, A. M.; Aivazian, G.; Yan, J.; Mandrus, D. G.; Xiao, D.; Yao, W.; Xu, X. Electrical control of neutral and charged excitons in a monolayer semiconductor. *Nat. Commun.* **2013**, *4*, 1474.
(52) Kormányos, A.; Burkard, G.; Gmitra, M.; Fabian, J.; Zólyomi, V.; Drummond, N. D.; Fal'ko, V. **k.p** theory for two-dimensional transition metal dichalcogenide semiconductors. *2D Mater.* **2015**, *2*, 022001.
(53) Brem, S.; Linderälv, C.; Erhart, P.; Malic, E. Tunable Phases of Moiré Excitons in van der Waals Heterostructures. *Nano Lett.* **2020**, *20*, 8534−8540.
(54) Wang, Z.; Chiu, Y.-H.; Honz, K.; Mak, K. F.; Shan, J. Electrical Tuning of Interlayer Exciton Gases in WSe_2 Bilayers. *Nano Lett.* **2018**, *18*, 137−143.
(55) He, Y.; Yang, Y.; Zhang, Z.; Gong, Y.; Zhou, W.; Hu, Z.; Ye, G.; Zhang, X.; Bianco, E.; Lei, S.; Jin, Z.; Zou, X.; Yang, Y.; Zhang, Y.; Xie, E.; Lou, J.; Yakobson, B.; Vajtai, R.; Li, B.; Ajayan, P.; et al. Strain-Induced Electronic Structure Changes in Stacked van der Waals Heterostructures. *Nano Lett.* **2016**, *16*, 3314−3320.
(56) Bai, Y.; et al. Excitons in strain-induced one-dimensional moiré potentials at transition metal dichalcogenide heterojunctions. *Nat. Mater.* **2020**, *19*, 1068−1073.

https://doi.org/10.1021/acs.nanolett.1c01207
Nano Lett. 2021, 21, 4461−4468

(57) Li, Z.; Wang, T.; Lu, Z.; Khatoniar, M.; Lian, Z.; Meng, Y.; Blei, M.; Taniguchi, T.; Watanabe, K.; McGill, S. A.; Tongay, S.; Menon, V. M.; Smirnov, D.; Shi, S.-F. Direct Observation of Gate-Tunable Dark Trions in Monolayer WSe_2. *Nano Lett.* **2019**, *19*, 6886−6893.
(58) Luo, Y.; Liu, N.; Kim, B.; Hone, J.; Strauf, S. Exciton Dipole Orientation of Strain-Induced Quantum Emitters in WSe_2. *Nano Lett.* **2020**, *20*, 5119−5126.
(59) Robert, C.; Lagarde, D.; Cadiz, F.; Wang, G.; Lassagne, B.; Amand, T.; Balocchi, A.; Renucci, P.; Tongay, S.; Urbaszek, B.; Marie, X. Exciton radiative lifetime in transition metal dichalcogenide monolayers. *Phys. Rev. B: Condens. Matter Mater. Phys.* **2016**, *93*, 205423.
(60) Castellanos-Gomez, A.; Buscema, M.; Molenaar, R.; Singh, V.; Janssen, L.; van der Zant, H. S.; Steele, G. A. Deterministic transfer of two-dimensional materials by all-dry viscoelastic stamping. *2D Mater.* **2014**, *1*, 011002.
(61) Psilodimitrakopoulos, S.; Mouchliadis, L.; Paradisanos, I.; Kourmoulakis, G.; Lemonis, A.; Kioseoglou, G.; Stratakis, E. Twist Angle mapping in layered WS_2 by Polarization-Resolved Second Harmonic Generation. *Sci. Rep.* **2019**, *9* (14285), 14285.
(62) Hsu, W.-T.; Zhao, Z.-A.; Li, L.-J.; Chen, C.-H.; Chiu, M.-H.; Chang, P.-S.; Chou, Y.-C.; Chang, W.-H. Second Harmonic Generation from Artificially Stacked Transition Metal Dichalcogenide Twisted Bilayers. *ACS Nano* **2014**, *8*, 2951−2958.

https://doi.org/10.1021/acs.nanolett.1c01207
Nano Lett. 2021, 21, 4461−4468